

Available online at www.sciencedirect.com

jmr&t
Journal of Materials Research and Technology
journal homepage: www.elsevier.com/locate/jmrt



Original Article

Influence of thermally grown oxides on interfacial friction during hot deformation of large-size forging ingots



Ali Vedaiei-Sabegh^a, Jean-Benoît Morin^b, Henri Champlaud^{a,*},
Mohammad Jahazi^a

^a École de Technologie Supérieure, Department of Mechanical Engineering, 1100 Notre-Dame Street West, Montreal, QC, H3C 1K3, Canada

^b Finkl Steel Inc., 100 McCarthy, Saint-Joseph-de-Sorel, QC, J3R 3M8, Canada

ARTICLE INFO

Article history:

Received 2 July 2022

Accepted 25 October 2022

Available online 28 October 2022

Keywords:

High-temperature oxidation

Nano-indentation

Ring test

FEM simulation

ABSTRACT

High-strength steels are pre-heated in gas-fired furnaces before undergoing the open-die forging process. This process increases thermal oxidation on steel surfaces, affecting the interfacial friction between ingot and anvils during deformation. Two medium carbon high-strength steels with different nickel contents were oxidized, and the mechanical characteristics of oxide layers were investigated by micro and nano-indentation methods. It was found that the formed layers on high nickel steel had lower Young modulus and hardness compared to the steel with lower nickel. Finite element modeling and ring tests were used to assess oxide layers' effect on interfacial friction during deformation. The results demonstrated that oxide layers' formation decreased the interfacial friction and deformation load, acting as lubricants at high temperatures.

© 2022 The Authors. Published by Elsevier B.V. This is an open access article under the CC BY-NC-ND license (<http://creativecommons.org/licenses/by-nc-nd/4.0/>).

1. Introduction

Thermally grown oxides can form on most steels during hot deformation by interacting solid with reactive gaseous atmosphere [1]. In addition to material waste and surface quality deterioration by oxidation, the interfacial condition can be influenced by scale layers. The presence of oxide can change the heat transfer between the ingot and the dies as well as the surrounding environment [2]. During deformation, the oxide layers can detach and break into the ingot, causing cracking

[3]. Also, friction and wear between the ingot and the dies can be affected by the presence of oxides, thereby decreasing their useful service time [4].

To form the oxide layers, the Fe ions must diffuse outward the surface. The oxidation kinetics is influenced by the diffusion of Fe ions (Fe^{2+} and Fe^{3+}) and inward diffusion of oxygen anions (O_2) [5]. Temperature and time are two factors increasing the diffusion of Fe and oxygen and increasing the kinetics of oxidation [6]. The thermally grown oxide on pure iron is comprised of three layers: wüstite (FeO), magnetite (Fe_3O_4), and hematite (Fe_2O_3) [7]. Wüstite is the first layer,

* Corresponding author.

E-mail address: henri.champlaud@etsmtl.ca (H. Champlaud).

<https://doi.org/10.1016/j.jmrt.2022.10.131>

2238-7854/© 2022 The Authors. Published by Elsevier B.V. This is an open access article under the CC BY-NC-ND license (<http://creativecommons.org/licenses/by-nc-nd/4.0/>).

closest to the base metal, with the lowest hardness between all scale layers. Hematite has the highest hardness, causing wear on contacting surfaces. Magnetite has an intermediate hardness compared to the two other layers [8]. The chemical composition of the alloy, oxidation atmosphere, oxidation time, and oxidation temperature all influence the diffusion of Fe and oxygen and, therefore, the thickness of the different scale layers [1].

For oxidation of low carbon steel at 1073–1423 K, Abulwefa et al. [9] observed all three scale layers by oxidation in pure oxygen. However, only a single wüstite layer was found for the oxidation of the same steel in the water vapor atmosphere. Si was found to decrease the oxidation of low alloy steel below 1450 K by Alaoui Mouayd et al. [10]. Takeda et al. [11], reported that Cr decreased the oxidation kinetics of low carbon steels by forming a FeOCr_2O_4 layer at the oxide-metal interface. Webler et al. [12] found that the addition of $0.3\text{Cu} + 0.1\text{Ni}$ decreased pure iron oxidation. Yin et al. [13] assessed Fe–Cu–Ni alloys' oxidation at 1423 K, where Ni increased the oxidation resistance. In a recent study, the effect of Ni on high temperature oxidation of high-strength steels was evaluated by Vedaei et al. [14]. The results showed a remarkable decrease in oxidation kinetics by adding Ni. However, the impact of the oxide layers on interfacial friction during high temperature deformation was not studied. Such evaluation would require accurate determination of the mechanical properties of the oxide layers.

Considering each oxide layer's different characteristics, the tribological conditions can be remarkably affected at the die-ingot interface [1]. Methods like ring test and pin on disk can be employed to investigate the oxide layer's effect on the friction between the die and the ingot. Hot ring compression test is a commonly employed method to evaluate the interface tribology at high temperature and obtain the variations in deformation loads and interfacial friction coefficient, accurately [15,16]. Ashimabha et al. [17] investigated the interface tribology of 316 L stainless steel using ring compression test in dry deformation condition. The rings were deformed in the temperature range of 1173–1473 K without considering the effect of thermal oxidation on interfacial friction. The authors reported higher friction at 1173 K and smaller at 1473 K and associated the obtained results to changes in different degrees of thermal softening and material flowability with temperature. Munther and Lenard [6] assessed the effect of oxide layers on the interfacial tribology during rolling of AISI 1018 steel and reported that the friction coefficient decreased by increasing the oxide thickness with the highest friction for 0.015 mm of scale and the lowest for 1.01 mm. Employing high temperature pin on disc method, Vergne et al. [18] investigated the effect of oxidation on interfacial tribology between AISI 1018 disc with a cast iron pin. It was found that oxidation at 1223 K for 1 h decreased both interfacial friction and wear. Zambrano et al. [19] used pin on the disk to assess the effects of oxide layers formed on ASTM A36 steel at 1223 K, against two high speed steels. The outcomes showed that the formation of oxides decreased the friction coefficient, whereas the wear rate increased. Graf et al. [20] used ring compression tests at 1173 and 1273 K for evaluation of friction and deformation load of C15 steel and reported that the presence of 30 and 50 μm of scale layers remarkably decreased the friction

and deformation load of rings. Hardell et al. [21] employed pin on disc to assess the influence of oxide formation on interfacial friction between two steels. It was found that the formation of higher amounts of magnetite layers at 673 K decreased the friction and wear rate between contacting surfaces. Odabas [22] investigated the interfacial tribology between AISI 3315 Steel against AISI 3150 Steel with pin on ring method. They reported lower interfacial friction on samples submitted to higher loads or sliding speeds and related their findings to higher temperatures at the surface, and hence oxidation, of such samples. Matsumoto et al. [23] used ring compression tests to investigate the oxide layer's tribological impact on the deformation of Cr rich steels at 1273 K and concluded that the presence of oxide layers with thickness in the range of 6–300 μm resulted in reduced deformation loads. However, in their simulations, the oxide layer was considered as a single layer of wüstite and very little microstructure analysis of the oxide material behavior was carried out.

The above studies show that the formation of thermal oxides reduces the interfacial friction during deformation. Therefore, accurate quantification of the impact of oxide layers requires a more precise determination of the mechanical and morphological characteristics of different oxide layers as a function of process parameters such as oxidation temperature, oxidation time, initial composition, or oxidation atmosphere. The evaluation of the above characteristics of different oxide layers and their different effects on interfacial friction is a piece of critical information that needs to be determined to accurately predict the friction coefficient. To acquire the mechanical properties of the different oxide layers, tensile or compression tests could be employed. However, these methods need molds, machining, furnaces, and complex sample preparations, making them time-consuming, and costly. Micro and nano-indentation methods are prevalent methods to investigate thin films and coatings and more convenient to conduct compared to compression tests. However, micro and nano-indentation test results are very sensitive to slight variations in oxidation temperature, oxidation time, oxidation atmosphere, or initial composition. For instance, Takeda et al. [24] measured at room temperature the hardness of formed oxide layers on pure iron at 1273 K. The Vickers hardness for wüstite, magnetite, and hematite was 3.5, 4, and 6.7 GPa, respectively. On the other hand, Barrau et al. [25] reported different hardness values, 2.64–2.94, 4.2–4.9, and 10.1 GPa for wüstite, magnetite, and hematite layers formed on iron, respectively. Luong and Heijkoop [26] obtained 4.6, 5.3, and 10.3 GPa for the three oxide layers formed on AISI 1340 steel oxidized at 1423 ± 20 K in air. Amano et al. [27] reported 3.5, 3.9, and 7.2 GPa values for the hardness of wüstite, magnetite, and hematite formed on Fe-0.5Si alloys at 1273 K for 18 ks in air and measured at room temperature. Zambrano et al. [8] investigated the hardness of different oxide layers formed at 1473 K in the air on a low carbon steel and obtained hardness values of 5.5 ± 1.1 , 6.5 ± 0.9 , and 12 ± 2.5 GPa for wüstite, magnetite, and hematite layers at room temperature. Hutchings and Shipway [28] reported a hardness range of 3.6–5.9 GPa for magnetite, for different oxidation conditions. The above studies reveal that the initial composition has a significant influence on the characteristics of each oxide layer and,

therefore, the need for conducting indentation tests for each specific steel. Finally, it must be noted that one of the factors that could also influence the reported results is the measurement technique (i.e., nano-indentation or micro-indentation), as evidence by results reported by Chicot et al. [29] and Seo and Chiba [30] on magnetite hardness values. Therefore, in the present study, both nano indentations and micro indentation techniques were used in order to ensure the accuracy of the obtained mechanical characteristics of the thermal oxides.

Although the indicated analysis shows the impacts of oxide layers on friction between die and ingot, very little information is available on the specific roles of different oxide layers and the evolution of their morphological and mechanical properties as a function of oxidation parameters. The aim of the present study is to investigate the characteristics of each oxide layer and assess the effect of oxidation on interfacial friction between ingot and anvil during open die forging. In this regard, oxidation experiments were carried out on two different high-strength steels at different temperatures, and the mechanical properties of each oxide layer was assessed employing micro and nano-indentation tests. The results were then employed as input for finite element simulations to evaluate oxide layers' effect on the interfacial friction between anvils and ingot using high-temperature ring tests to simulate the open die forging process.

2. Materials and methods

Two high-strength medium carbon low alloy steels were used in the present study. One of the sub-objectives of the project was to evaluate the impact of a higher Ni content on the oxidation behavior of large size components during open die forging, and therefore a higher Ni content was employed, as shown in Table 1. For ease of use, the steels are identified as low nickel (LNi) and high nickel (HNi). The materials were provided by Finkl steel, Sorel, Quebec, Canada, and were obtained from large-size forgings used in energy and transportation industries.

2.1. Oxidation experiments

Samples for the oxidation experiments were cylinders with 10 mm diameter and 15 mm height. Before oxidation experiments, the samples were grounded by 320 mesh SiC papers to achieve similar surface roughness and ultrasonically cleaned and kept in the vacuum chamber. The oxidation tests were conducted employing a radiative furnace mounted on a Material Testing System (MTS), series 809. The furnace was a water-cooled IR E4 Research Inc. radiative type and was

equipped with four lamps and elliptical polished aluminum reflectors that provided the infrared radiation and produced a hot zone with uniform temperature over a 100 mm distance thereby, producing uniform temperature conditions all around the samples. Samples were heated to an oxidation temperature of 1473 K with a heating rate of 2 K/s. The heating was conducted under the protection of argon gas with a flow rate of 50 ml min⁻¹ to avoid oxidation during heating. At this temperature, the argon was switched off for 60 min, leaving the sample to oxidize in the air. Then, the argon flow was connected again to cool down the sample to room temperature and avoid oxidation during cooling. The formed scale layers are fragile and need to be carefully preserved for metallography, indentation, and microscopy. A method was developed to guard the scale layers from manipulation damages. This method consisted of using a cold mounting product composed of 60–70% Zirconium oxide, 20–40% fused Silica and 0–10% Aluminum oxide with a hardener composed of Amines, polyethylenepoly, and triethylenetetramine and introduced to the oxidized sample in a vacuum chamber. As thermal oxidation is a surface phenomenon, it is reigned by the diffusion of ions near the surface. So, the oxide growth would be the same for a small sample compared to a large-sized ingot.

2.2. Indentation on oxide layers

To evaluate the material properties of different scale layers, indentation tests were conducted. Micro-indentation tests were conducted using an Anton Paar Micro-Hardness Tester (MHT), and nano-indentation tests were carried out with Micromaterials NanoTest Vantage. For both tests, a Vickers diamond indenter was used on the transverse section of oxide layers. Before nano-indentation, the sample was placed in the machine chamber for 48 h to ensure temperature homogeneity. The diamond tip was applied to the examination point up to a specific load during the indentation, where it was kept for 30 s, followed by unloading [31]. The output of an indentation test is a curve showing the applied load versus the indentation depth. The contact depth of the indenter, h_c , was calculated using the Oliver and Pharr analysis [32,33]:

$$h_c = h_m - \epsilon \frac{F_m}{S} \quad (1)$$

where h_m is the maximum indentation depth (μm), ϵ is a constant related to the indenter geometry, F_m the maximum normal load (mN), and S is the stiffness of the sample (mN/ μm) acquired from the slope of the unloading portion of the indentation curve. In the unloading part of the graph, the instrumented hardness of the tested material, H_{IT} , can be obtained using equation (2) [32,33]:

$$H_{IT} = \frac{F_m}{A_p} \quad (2)$$

where A_p is the contact area between the indenter and the specimen at the maximum depth and load (μm^2). Reduced elastic modulus, E_r (GPa), considers that the elastic displacement occurs in both indenter and sample and can be obtained as follows [32,33]:

Table 1 – Chemical composition of employed steels (wt%).

	C	Mn	Si	Ni	Cr	Mo	Cu
LNi	0.35	0.99	0.41	0.5	1.86	0.53	0.16
HNi	0.35	0.99	0.41	2.92	1.86	0.53	0.16

$$E_r = \frac{\sqrt{\pi} S}{2\beta \sqrt{A_p}} \tag{3}$$

where β is a geometrical constant on the order of unity. The instrumented elastic modulus in the specimen, E_{IT} , is acquired as follow [32,33]:

$$\frac{1}{E_r} = \frac{(1 - \nu_s^2)}{E_{IT}} + \frac{(1 - \nu_i^2)}{E_i} \tag{4}$$

where ν_s is the Poisson's ratio of specimen and E_i and ν_i are the elastic modulus and Poisson's ratio of the indenter, which for a diamond indenter are 1141 GPa and 0.07 [34].

2.3. Hot compression tests

To obtain the stress-strain behavior of the studied materials for friction assessment, hot compression tests were conducted. Cylindrical samples 10 mm diameter and 15 mm height were heated to 1373 and 1473 K under argon protection to avoid oxidation and compressed to 50% of their height. The strain rate was 0.25 s^{-1} , which is designated based on the employed parameters of the industrial partner for this study. To minimize the effect of friction on results, graphite powder and mica sheets were placed between the sample and the anvils. However, a slight barreling was still observed, indicating some friction during compression testing. Therefore, the stress-strain curves were corrected for this frictional effect to ensure accurate evaluation of the material mechanical behavior during high-temperature deformation. The instantaneous friction was calculated as follows [35]:

$$\mu = \mu_0 + A \exp\left(\frac{\epsilon}{\epsilon_0}\right) \tag{5}$$

where μ_0 , A, and ϵ_0 are constants and are given in Table 2 for different temperatures based on empirical investigations [35]. Using equation (5) and the data in Table 2, the corrected stress related to the deformation can be calculated as follows [35]:

$$\sigma = \frac{C^2 P}{2[\exp(C) - C - 1]} \tag{6}$$

with $C = \frac{2\mu r}{h}$ (7)

where P is the acquired stress from the testing device, r and h are the specimen's initial radius and height.

2.4. Hot ring compression test for friction assessment

Originated by Kunogi [36] and improved in a practical way to be utilized by Male and Cockcroft [37], ring test is an accurate method to obtain the friction coefficient. This method is commonly used for the determination of interfacial friction

coefficient on various materials, including steels [15,16,38]. Rings with dimensions of 18 mm for outer diameter, 9 mm inner diameter, and 6 mm height were machined from the as-received materials. These rings were heated to 1373 and 1473 K deformation temperatures and isothermally deformed to 50% of their height. The variation of the ring inner diameter with the height reduction can be correlated with the friction at the die-part interface [39]. If the friction is low, the ring will flow outwards, causing the inner diameter to increase. If the friction is high, the material will flow inward, and the inner diameter will decrease.

The rings were oxidized before deformation to evaluate thermal oxidation's effect on the interfacial friction during deformation. Before compression testing, the rings were hung with the help of a support inside the furnace to allow both parallel surfaces of the sample to be in contact with the air and be oxidized by the indicated procedure in section 2.1. Two oxidation temperatures, 1373 and 1473 K, and three oxidation times, 10, 30, and 60 min, were used to assess the influence of different oxide thickness on interfacial friction.

3. Finite element modeling of the ring test

Friction calibration curves (FCC), as reported in the literature [39], have been widely employed to estimate the friction coefficient by obtaining the variation of inner diameter for a specific height reduction. However, the studies have demonstrated that the FCCs can be remarkably different for various materials, deformation temperature, heat transfer, ring geometry, etc. [39]. In other words, the utilization of conventional FCCs cannot be a precise approach for all investigations. On the other hand, experimental determination of FCC for all the experimental conditions encountered in actual deformation processing conditions is a very time-consuming exercise; hence, finite element (FE) with Abaqus/CAE software was used to develop each of the investigated steels' FCC. Due to the axisymmetric nature of the ring-compression test, a 2D axisymmetric model was developed. Furthermore, because of the planar symmetry during compression, half of the ring's cross-section was considered in the simulations, which further reduced the computational time during the simulations. The die was considered as a non-deformable discrete rigid with 2-node linear axisymmetric rigid elements (RAX2). The ring was modeled as deformable elastic-plastic with 4-node bilinear axisymmetric quadrilateral mesh (CAX4R) for axisymmetric stress. The mechanical properties were acquired by the cylindrical compression tests. Rings were deformed up to 60% of the height. Fig. 1 shows the employed mesh and deformation of the LNi ring at 1473 K. Based on the machine manual, the die temperature was considered the same as the ring, as the temperature is uniform for 100 mm length inside the radiative furnace, taking the advantage of long radiative lamps and reflectors. This assumption was verified by installing a thermocouple on die surface during oxidation, where the discrepancies between ring and die temperature were negligible. The ring could deform in both horizontal and vertical directions, whereas the die had the freedom to only move in a vertical direction.

Table 2 – Employed constants for friction correction [35].

Temperature (K)	μ_0	A	ϵ
1373 K	0.3002	0.07844	0.61564
1473 K	0.3935	0.02739	0.42256

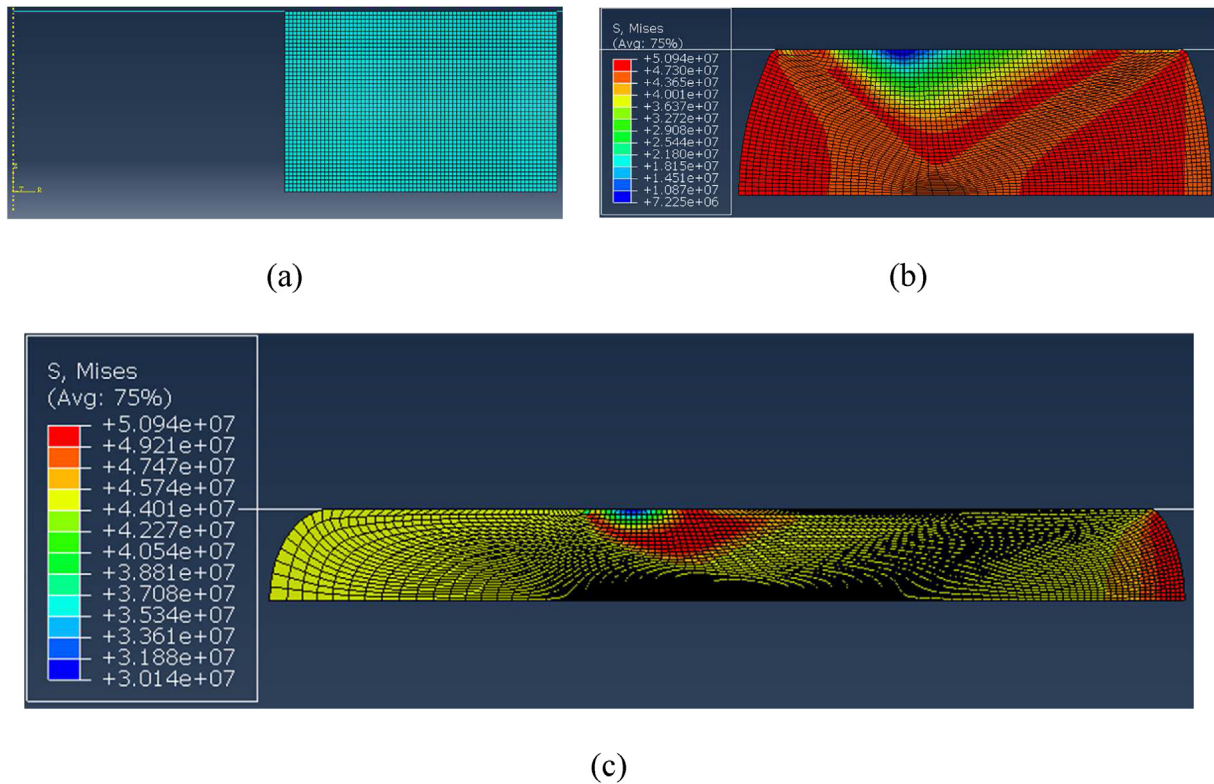


Fig. 1 – a) Developed 2D axisymmetric FE model of ring for deformation, b) 45% compression of LNi ring at 1473 K, and c) 60% compression of LNi ring at 1473 K.

The two common friction models utilized in metal forming to describe the frictional conditions of contacting surfaces are the Coulomb friction model and the constant shear friction law [40]. These models can be indicated as follows [41,42]:

$$\tau = \mu P \text{ (Coulomb friction model)} \quad (8)$$

$$\tau = mK, K = \frac{\sigma_s}{\sqrt{3}} \text{ (Constant shear friction law)} \quad (9)$$

where τ , μ , P , m , and σ_s are frictional shear stress, friction coefficient, normal stress, shear friction factor, and effective flow stress [41,42]. The FCCs in this study are developed by both models to understand better and compare two friction models.

4. Results and discussion

4.1. Micro-indentation and nano-indentation on oxide layers

Fig. 2 shows the formed oxide layers on LNi and HNi steel at 1473 K for 60 min. The three oxide layers of hematite at the top, magnetite as an intermediary layer, and wüstite at the bottom can be seen for both steels. The formed scale layers on HNi are thinner compared to LNi steel, as Ni suppressed the oxidation. The formed oxide sub-layers, and the mechanism by which Ni hinders the oxidation were discussed in a former study [14]. The formed thermal oxide on HNi steel is

continuous and smooth compared to the rough and porous LNi ones, particularly for the magnetite layer. Furthermore, the interface of oxide-metal for grown oxide layers on HNi steel is thicker, which implies the better adhesion of this scale to the base metal compared to LNi one. Despite the presence of pores and cracks during sample preparation, there was still sufficient room to conduct indentation tests properly.

The Vickers micro indenter was applied to different oxide layers, leaving a pyramid with square base imprint (see Fig. 3). The indenter was applied with different loads, held for 30 s at peak load and followed by unloading, as illustrated in Fig. 4-a for formed wüstite on LNi steel at 1473 K. The evolution of the penetration depth for indenter as a function of indentation load is shown in Fig. 4-b.

Employing Fig. 4-a and 4-b with equations (1)–(4), the Young modulus and hardness of different oxide layers were determined according to Oliver and Pharr's method [32,33]. The results for the formed wüstite layer on both steels are given in Fig. 5. The results reveal that the average Young modulus of wüstite formed on LNi steel and acquired with micro-indentation was 141.0 ± 7.5 GPa while the one for the HNi steel was remarkably lower, at 100.0 ± 6.0 GPa. It is interesting to note that the Young modulus's results obtained from nano-indentation of the LNi sample are very close to the ones obtained by micro indentation 145.5 ± 3.5 GPa. This finding indicates the reliability of the less demanding micro-indentation technique as compared to the more complex experimental set-up of the nano-indentation one for characterizing oxide layers.

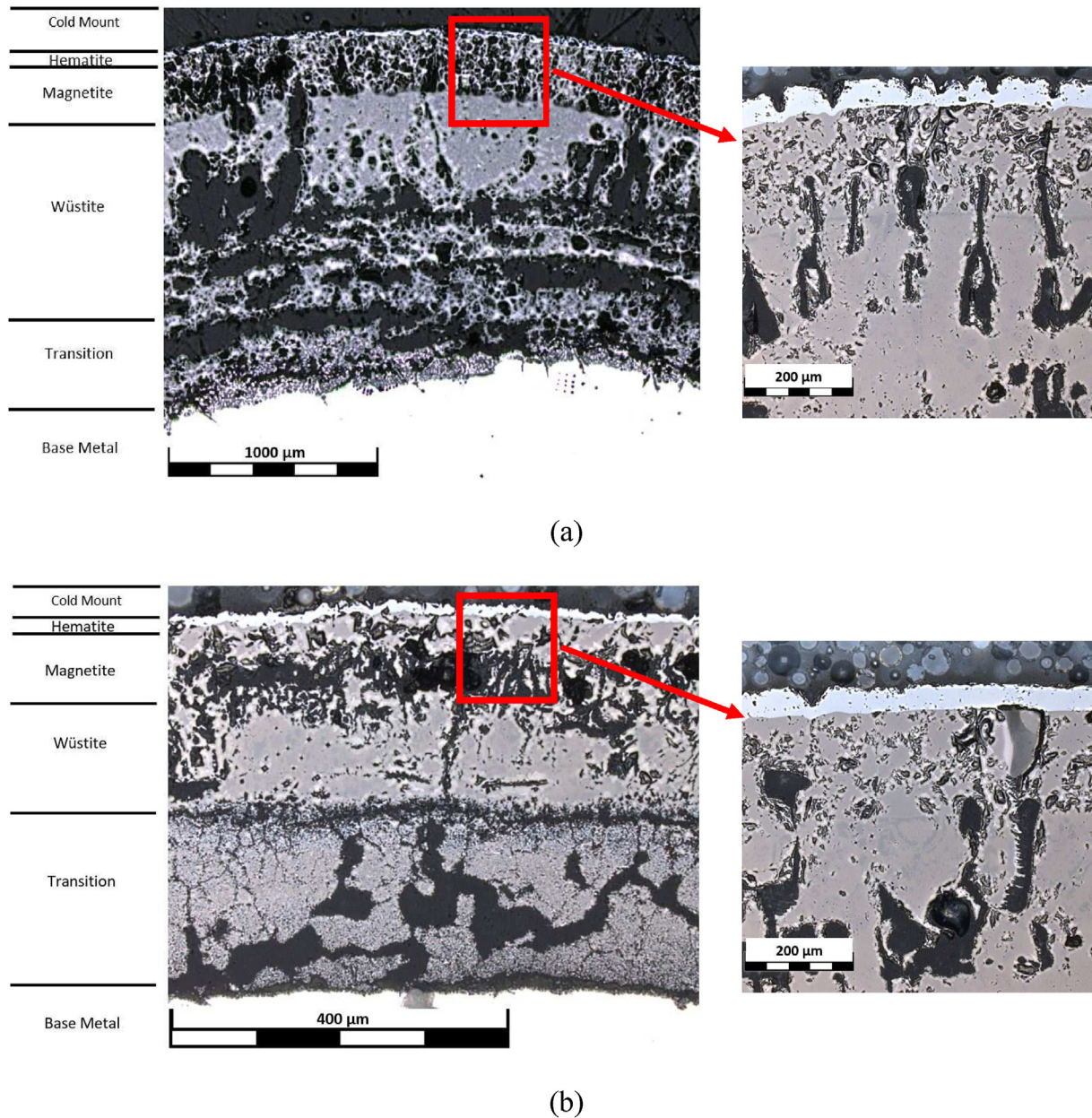


Fig. 2 – Formed thermal oxide layers: a) LNi steel at 1473 K for 60 min, and b) HNi steel at 1473 K for 60 min.

The hardness of wüstite on LNi was determined to be 6.0 ± 0.3 GPa by both micro and nano-indentation techniques, further confirming the reliability of measures with micro-indentation technique. It is also interesting to note that the hardness of the wüstite layer on the HNi steel was about 3.7 ± 0.3 GPa which is much softer than the one in measured in the LNi steel. The results also show that the stiffness of wüstite increases by increasing the applied load or penetration depth. The elastic-plastic work conducted to penetrate both wüstite layers on steels was equal to %26 and %74 for elastic work and plastic work, respectively. The elastic and plastic work are total conducted work units during indentation, which equal to the area under indentation force-penetration depth curve (see Fig. 4-b). The elastic and plastic

work are the area under unloading and loading parts of curve, respectively [43]. In agreement with the Young modulus results, the stiffness of the wüstite for LNi steel was higher than that of the HNi steel.

The results for the formed magnetite layer on LNi and HNi steels are illustrated in Fig. 6. The average elastic modulus of the magnetite layer acquired by micro-indentation and nano-indentation were 160.0 ± 6.0 GPa and 162.0 ± 5.3 GPa, respectively. A lower value of 143.0 ± 8.6 GPa was measured for the Young modulus for the magnetite layer grown on HNi steel. The same trend was observed for hardness as the hardness of magnetite on LNi was 6.0 ± 0.2 GPa, obtained from both micro and nano-indentation, compared to 5.0 ± 0.4 GPa of hardness for the layer on HNi steel. The stiffness for formed magnetite

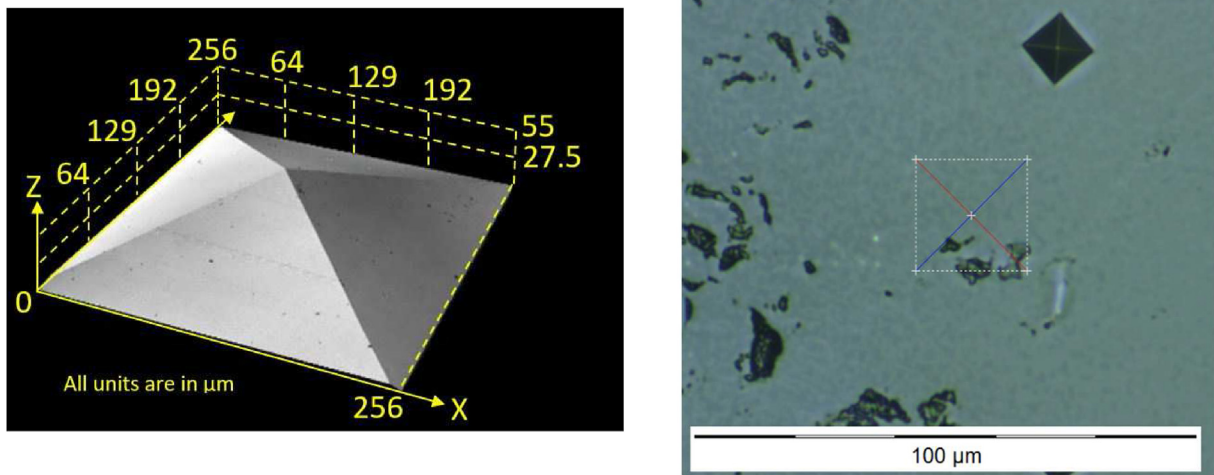


Fig. 3 – The utilized Vickers indenter tip (LEXT microscopic image-left) and the imprint obtained on the oxide layer (right).

on LNi was slightly higher compared to the one on HNi. Still, the same percentage of %26 and %74 was observed for elastic and plastic work of both steels' magnetite.

Fig. 7 gives the results for the outermost layer, hematite formed on both steels. The Young modulus reached 236.0 ± 10.7 GPa and 239.0 ± 14.3 GPa acquired by micro and nano-indentation, further confirming the agreement between the measures made by both techniques. This value was remarkably lower at 195.0 ± 13.4 GPa for hematite of HNi steel. The same trend was observed for hardness as it was 11.0 ± 0.8 GPa and 13.7 ± 0.4 GPa for LNi compared to 8.8 ± 1.0 GPa for HNi one. Like the magnetite layer, LNi hematite's stiffness was slightly higher than grown hematite on HNi steel. The elastic and plastic work ratio was different from the previous two layers, equaling %42 and %58, respectively.

As the deformation occurs at high temperatures, the question can arise that will the measured Young modulus difference for formed oxide layers at room temperature can be seen at high temperature? The reported literature shows that the same type of difference is to be expected for the measured Young modulus at room temperature for high temperatures.

The conducted study by Schütze et al. [44] reported the following equation for obtaining the Young modulus at high temperature from measured amounts at room temperature:

$$E_{ox} = E_{ox}^0 (1 + n(T - 25)) \quad (10)$$

where E_{ox} is the Young modulus at high temperature (GPa), E_{ox}^0 is the Young modulus at room temperature (GPa), n is a constant which reported to be -4.7×10^{-4} for iron oxides, and T is designated temperature (K). Applying this equation to this case indicates that the difference between two thermally grown oxides will still be present at high temperature.

Based on equation (10), the 141 and 100 GPa of Young modulus for formed wüstite on LNi and HNi steels, decreases to 45 and 32 GPa (the same 40% difference) at 1473 K. For magnetite formed on LNi and HNi, the Young modulus is 51 and 46 GPa at 1473 K, compared to 160 and 143 GPa at room temperature. For hematite, the formed layer on LNi and HNi steels have the Young modulus of 236 and 195 GPa at room temperature, which is 75 and 62 GPa at 1473 K, employing the indicated equation (10). The same trend is observed for other high temperatures.

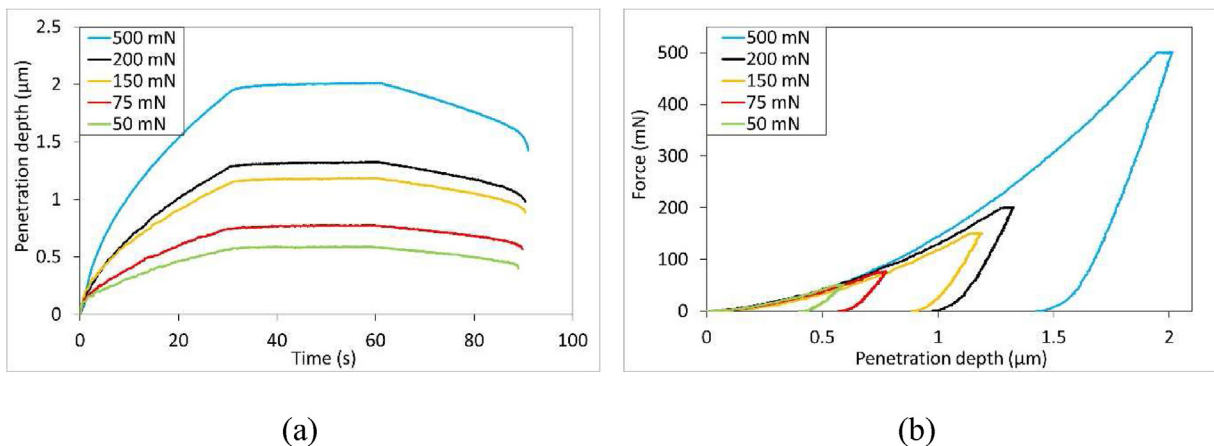


Fig. 4 – Indentation curves of formed wüstite on LNi steel at 1473 K: a) penetration depth of indenter for different loads by time, and b) different applied indentation loads for penetration depth.

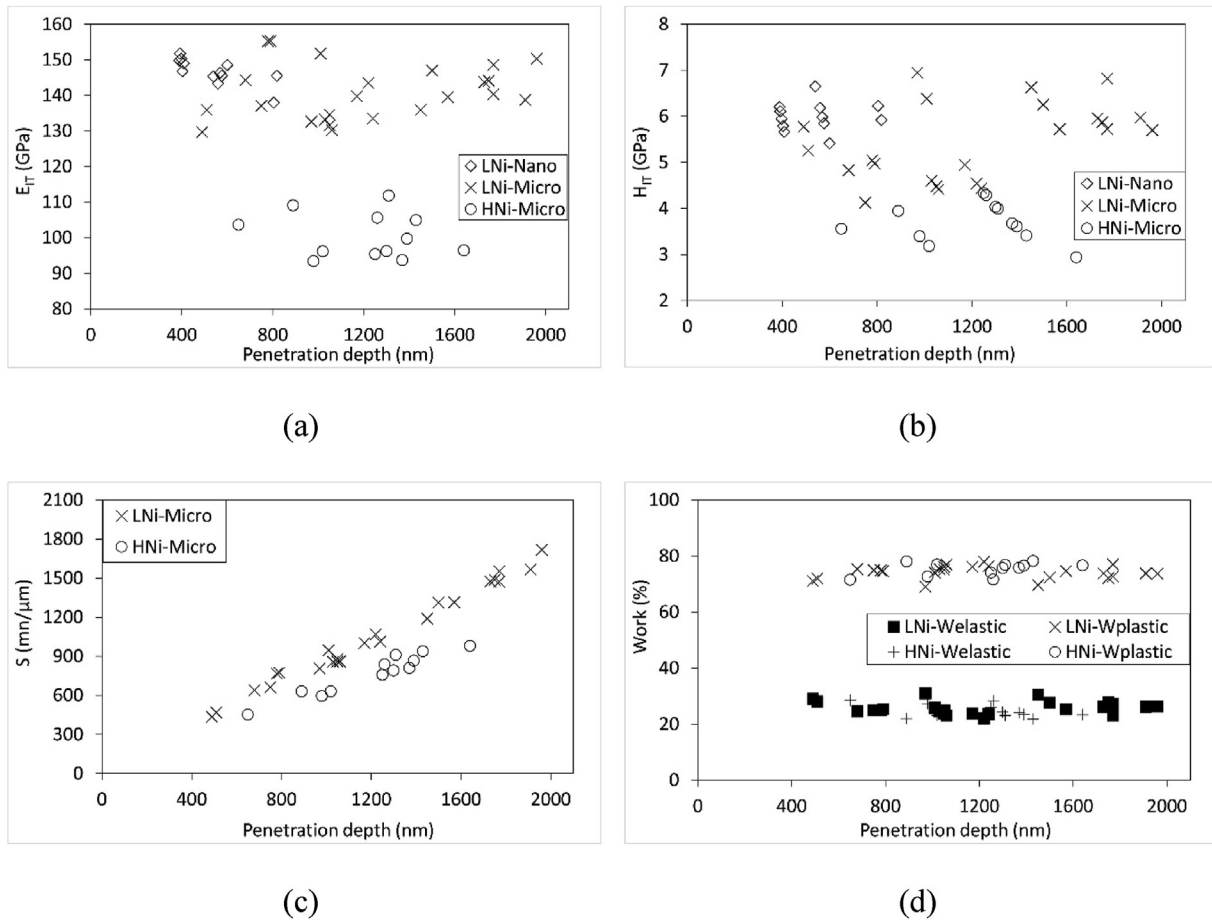


Fig. 5 – The indentation results on the wüstite layer formed on both LNi and HNi steels: a) elastic modulus, b) hardness, c) stiffness, and d) work.

The oxide-metal interface, known as the transition layer, is thicker for HNi steel compared to LNi. The thicker transition layer makes a better oxide-metal mechanical bonding, resisting for descaling of formed oxide on HNi steel. This case was evident during the cleaning of the samples from oxides. The formed oxide on LNi was cleared by a small force, whereas the HNi oxide needed a sharp edge and a higher force to remove. Micro-indentation on the transition layer showed that the hardness was 5.1 and 4.7 GPa for LNi and HNi steel, where the thicker layer has a lower hardness. Immediately after the transition layer, the micro-indentation measures on the base metal indicated a hardness of 3.7 and 2.9 GPa for LNi and HNi, respectively. The low hardness level of the base metal in the zone adjacent to the oxide-metal interface, is due to the decarburization by diffusion of ions. The above results clearly reveal the differences in the mechanical properties of the different layers and, therefore, the need for the quantification of their effects on the interfacial friction between ingot and anvils during deformation.

4.2. Friction calibration curves (FCCs)

As illustrated in Fig. 8, both steels' stress-strain curves were obtained by compression tests at 1373 and 1473 K with 0.25 s^{-1} , and the effect of friction was corrected using the

procedure described above. The corrected stress-strain curves were utilized for FE simulation of hot ring compression tests to develop the FCCs. The FCCs illustrated in Fig. 9 for LNi, and HNi steels were acquired at indicated temperatures of 1373 and 1473 K, by obtaining the variations of the inner diameter of rings by height reduction. The curves were acquired by both Coulomb and friction Constant shear friction models to provide a comparison between two models. The single points on the graphs show the results of the experimental tests for rings, with and without oxide layers, which makes the correlation between FE and experimental parts.

The results show that both friction models came to the same predictions for a friction coefficient range from frictionless conditions to a friction coefficient of $m = 0.2$. Afterward, the Coulomb model shows slightly higher values. However, the friction coefficient for conducted experiments never surpasses the coefficient of $m = 0.2$. For all tested conditions, the highest friction was obtained for rings without oxidation, at $m = 0.2$. At these temperatures, steel tends to stick to die surfaces and high frictional conditions are produced. The decrease in friction coefficient with the oxidation progress shows that the oxide layers act as a lubricant at high temperatures. For LNi, at deformation temperature of 1473 K, the friction decreased from $m = 0.2$ for the ring without oxidation to $m = 0.14$, 0.11 , and 0.1 after oxidizing the ring for

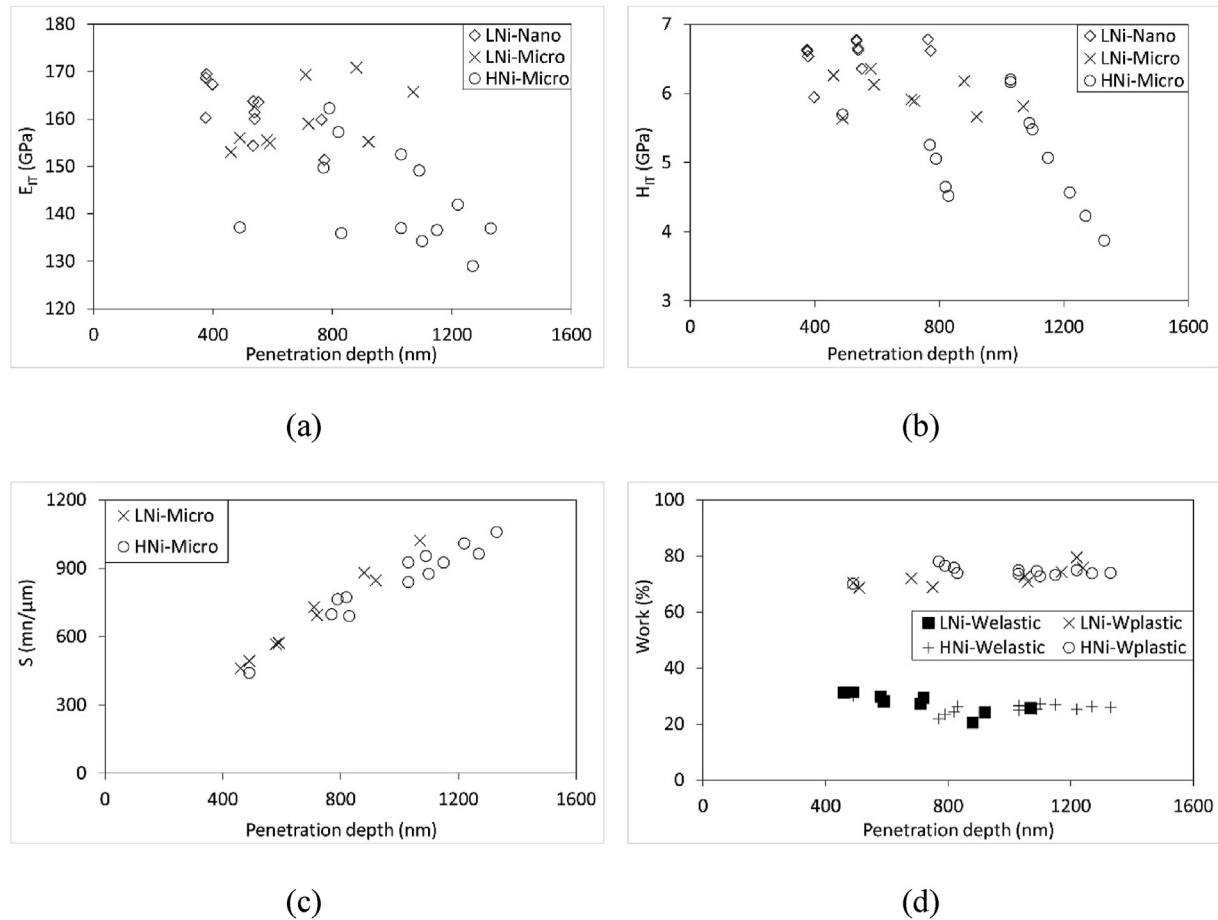


Fig. 6 – The indentation results on the magnetite layer formed on both LNi and HNi steels: a) elastic modulus, b) hardness, c) stiffness, and d) work.

10, 30, and 60 min, respectively. Therefore, as the oxide thickness increases, it can act more as a lubricant to decrease the ring and anvils' interfacial friction. This outcome is in accordance with the conducted studies by Zambrano et al. [45] on the tribological behavior of a mottled cast iron sliding against formed oxide on ASTM A36. Their results indicated that by increasing the testing temperature the friction coefficient decreases due to the formation of oxide layers. For HNi steel, at the same deformation temperature, the friction decreased from $m = 0.2$ to $m = 0.17$, 0.14 , and 0.12 for the 10, 30, and 60 min oxidation times, respectively. The friction decreased by oxidation for HNi steel, but at a lower level as compared to LNi steel. This issue is due to the lower thickness of the formed oxide on HNi steel than LNi steel, where the Ni modifies the oxidation. For LNi steel at deformation temperature of 1373 K , the friction coefficient was $m = 0.16$, 0.14 , and 0.12 by oxidation for 10, 30, and 60 min. For the same deformation temperature and oxidation times, friction coefficients of $m = 0.19$, 0.15 , and 0.13 were obtained for HNi steel. The results reported in Figs. 5–7 show that the Young modulus and hardness of the oxide layers formed on the LNi steel are higher than the ones on HNi steel. The higher mechanical properties of oxides on LNi samples, delays the early

disintegration of these layers. As these layers play the role of lubricants; therefore, the oxide layers of LNi steel decreased friction in a larger degree compared to the HNi oxides. This effect was further accentuated as the oxide layer on LNi was about 20% thicker than the one formed on the HNi one. As a result of friction decrease by oxide layers, the forming loads decrease too. Fig. 10 illustrates the applied forming loads by the anvils to deform rings, with and without oxide layers, at 1473 K . The required deformation loads for deformation of rings at 1473 K for both LNi and HNi steels were decreased by oxidation. This is related to the fact that oxide layers act as lubricants at this temperature. The loads for deformation of LNi steel decreased from 20412 N for without oxidation condition to 16815 , 15714 , and 14121 N after oxidation for 10, 30, and 60 min. For HNi steel, the deformation load decreased from 19677 N at its maximum to 17589 , 15975 , and 14874 N after oxidation for 10, 30, and 60 min. To validate the accuracy of the developed FE model and FCCs, the developed FE model was compared with the conducted experiments. The outer diameter of the ring after deformation, and the deformation load of the ring with respect to its height reduction were compared. The obtained results are in a reasonable agreement, and the errors are given in Fig. 11.

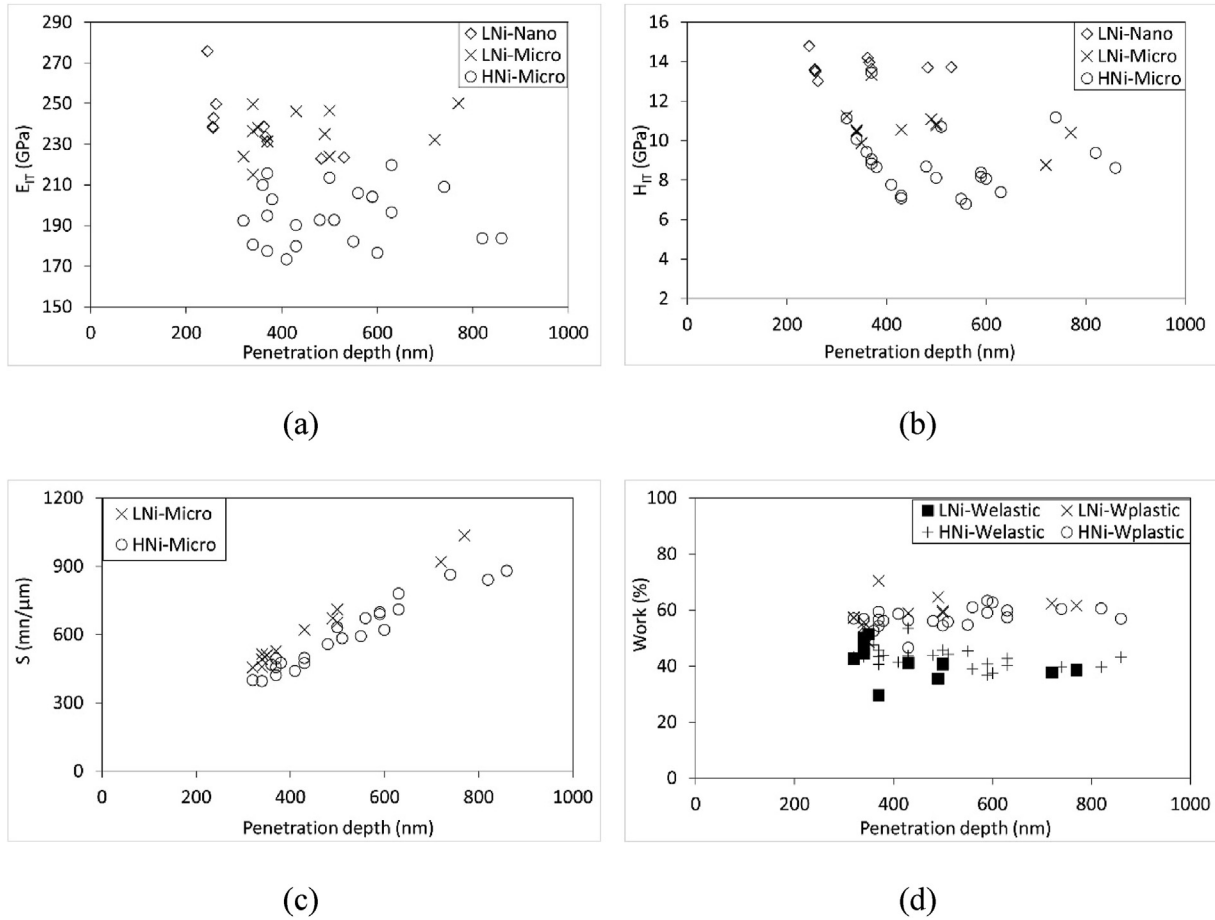


Fig. 7 – The indentation results on the hematite layer formed on both LNi and HNi steels: a) elastic modulus, b) hardness, c) stiffness, and d) work.

5. Summary and conclusions

The mechanical characteristics of different oxide layers formed on two high-strength steels were evaluated by micro-indentation and nano-indentation methods. It was found that while the same layers of wüstite, hematite, and magnetite

were observed for both steels, their characteristics were different. The micro-indentation and nano-indentation results on thermally grown oxide layers on LNi steel were close and in a reasonable agreement. The Young modulus, hardness and stiffness of all oxide layers were higher for formed layers on LNi steel than HNi ones, whereas the elastic and plastic work ratios remained the same for two oxides. The Young

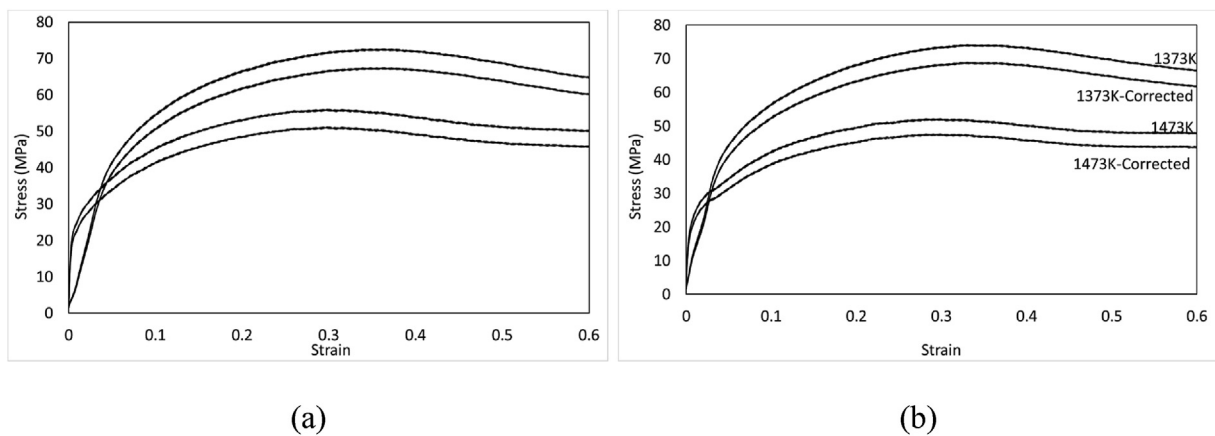


Fig. 8 – Acquired stress-strain curves from hot compression tests, and corrected for friction effects to be employed in FE simulation of ring tests, for: a) LNi, and b) HNi.

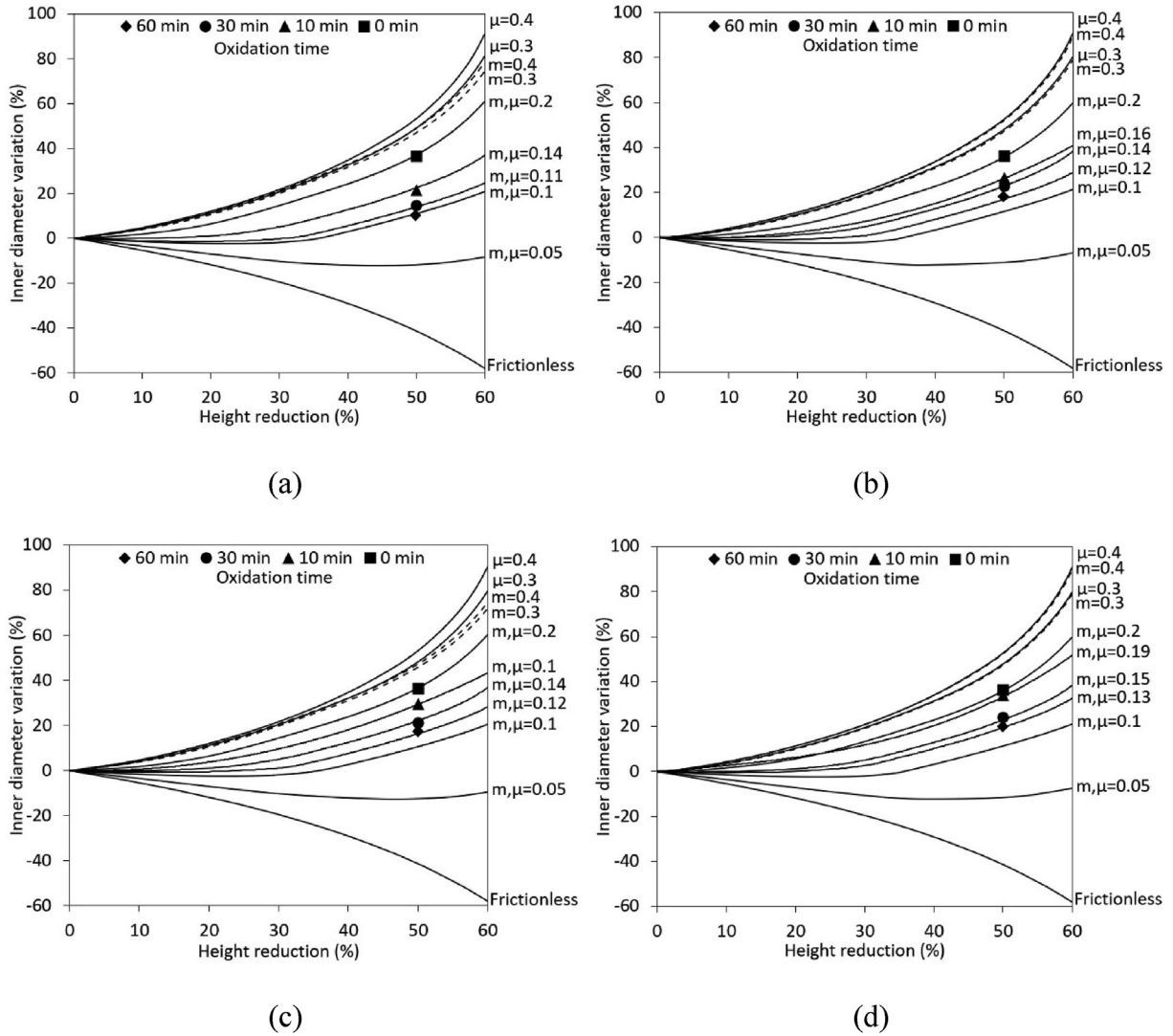


Fig. 9 – Acquired FCCs by variation of the inner diameter of the ring to its height reduction, with Coulomb and Constant shear friction models for: a) LNi at 1473 K, b) LNi at 1373 K, c) HNi at 1473 K, and d) HNi at 1373 K.

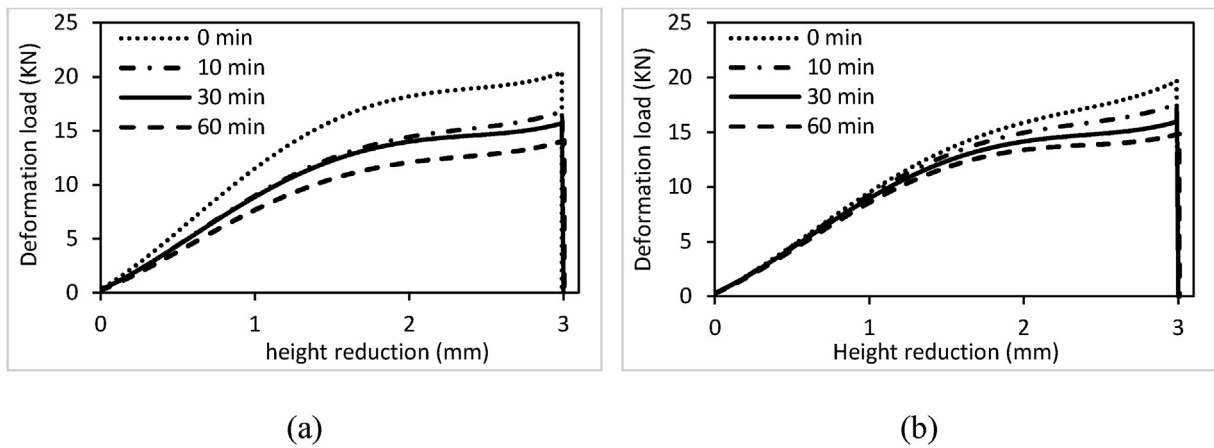


Fig. 10 – Acquired deformation loads from MTS by height reduction of rings at 1473 K, and different oxidation times, for: a) LNi, and b) HNi.

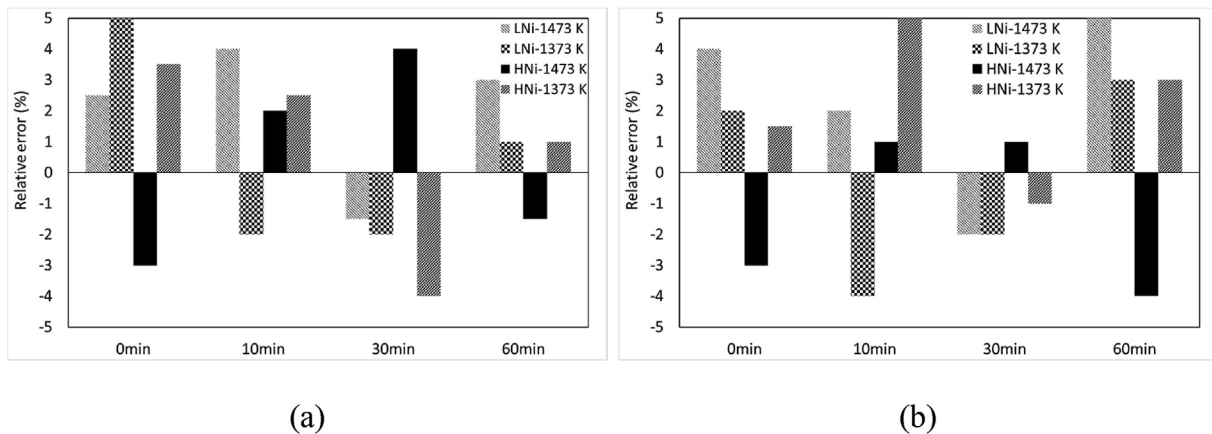


Fig. 11 – Relative error of the difference between developed FE model and conducted experimental tests for: a) outer diameter of the ring after deformation, and b) deformation load of ring with respect to its height reduction.

modulus and hardness values of LNi oxide layers were consistently higher than those for the HNi oxide layers. Ring compression tests and FEM modeling were employed to evaluate interfacial friction using both Coulomb and constant shear friction models. The results clearly showed that the presence of the oxide layer acted as a lubricant at higher temperatures with the oxide layers on LNi steel decreasing the friction more than the formed oxides on HNi steels. This phenomenon was associated with the higher thickness of formed oxide layers on LNi steel and the higher mechanical properties of LNi oxides compared to the HNi ones.

Declaration of Competing Interest

The authors declare the following financial interests/personal relationships which may be considered as potential competing interests:

Mohammad Jahazi reports financial support was provided by Natural Sciences and Engineering Research Council of Canada (NSERC).

Acknowledgment

The authors would like to express their appreciation to Finkl Steel for the current study's specimen supply. The authors would also like to thank Dr. Daniel Paquet at Institut de recherche d'Hydro-Québec (IREQ) for collaboration in conduction of indentation tests. This work was supported by the Natural Sciences and Engineering Research Council of Canada (NSERC) for their support in the framework of a Collaborative Research and Development project (CRD) [Grant number 5364418].

REFERENCES

- [1] Birks N, Meier GH, Pettit FS. Introduction to the high temperature oxidation of metals. Cambridge University Press Cambridge; 2006. <https://doi.org/10.1017/CBO9781139163903>.
- [2] Jang JH, Lee DE, Kim MY, Kim HG. Investigation of the slab heating characteristics in a reheating furnace with the formation and growth of scale on the slab surface. *Int J Heat Mass Tran* 2010;53:4326–32. <https://doi.org/10.1016/j.ijheatmasstransfer.2010.05.061>.
- [3] Utsunomiya H, Doi S, Hara K-i, Sakai T, Yanagi S. Deformation of oxide scale on steel surface during hot rolling. *CIRP Ann* 2009;58:271–4. <https://doi.org/10.1016/j.cirp.2009.03.050>.
- [4] Barrau O, Boher C, Gras R, Rezai-Aria F. Analysis of the friction and wear behaviour of hot work tool steel for forging. *Wear* 2003;255:1444–54. [https://doi.org/10.1016/S0043-1648\(03\)00280-1](https://doi.org/10.1016/S0043-1648(03)00280-1).
- [5] Suárez L, Rodríguez-Calvillo P, Houbaert Y, Colás R. Oxidation of ultra low carbon and silicon bearing steels. *Corrosion Sci* 2010;52:2044–9. <https://doi.org/10.1016/j.corsci.2010.02.001>.
- [6] Munther PA, Lenard JG. The effect of scaling on interfacial friction in hot rolling of steels. *J Mater Process Technol* 1999;88:105–13. [https://doi.org/10.1016/S0924-0136\(98\)00392-6](https://doi.org/10.1016/S0924-0136(98)00392-6).
- [7] Suárez L, Houbaert Y, Eynde XV, Colás R. High temperature deformation of oxide scale. *Corrosion Sci* 2009;51:309–15. <https://doi.org/10.1016/j.corsci.2008.10.027>.
- [8] Zambrano OA, Coronado JJ, Rodríguez SA. Mechanical properties and phases determination of low carbon steel oxide scales formed at 1200°C in air. *Surf Coat Technol* 2015;282:155–62. <https://doi.org/10.1016/j.surfcoat.2015.10.028>.
- [9] Abuluwefa HT, Guthrie RIL, Ajersch F. Oxidation of low carbon steel in multicomponent gases: Part I. Reaction mechanisms during isothermal oxidation. *Metall Mater Trans A* 1997;28:1633–41. <https://doi.org/10.1007/s11661-997-0255-7>.
- [10] Alaoui Mouayd A, Koltsov A, Sutter E, Tribollet B. Effect of silicon content in steel and oxidation temperature on scale growth and morphology. *Mater Chem Phys* 2014;143:996–1004. <https://doi.org/10.1016/j.matchemphys.2013.10.037>.
- [11] Takeda M, Kushida H, Onishi T, Toyama M, Koizumi F, Fujimoto S. Influence of oxidation temperature and Cr content on the adhesion and microstructure of scale on low Cr steels. *Oxid Metals* 2010;73:1–13. <https://doi.org/10.1007/s11085-009-9167-9>.
- [12] Webler B, Yin L, Sridhar S. Effects of small additions of copper and copper + nickel on the oxidation behavior of iron. *Metall Mater Trans B* 2008;39:725. <https://doi.org/10.1007/s11663-008-9196-9>.
- [13] Yin L, Balaji S, Sridhar S. Effects of nickel on the oxide/metal interface morphology and oxidation rate during high-

- temperature oxidation of Fe–Cu–Ni alloys. 41:598–611, <https://doi.org/10.1007/s11663-009-9334-z>; 2010.
- [14] Vedaiei-Sabegh A, Morin J-B, Jahazi M. Influence of nickel on high-temperature oxidation and characteristics of oxide layers in two high-strength steels. *Steel Res Int* 2020;91:1900536. <https://doi.org/10.1002/srin.201900536>.
- [15] Altan T, Ngaile G, Shen G. *Cold and hot forging: fundamentals and applications*. ASM international; 2004.
- [16] Dieter GE, Kuhn HA, Semiatin SL. *Handbook of workability and process design*. A S M International; 2003.
- [17] Ashimabha B, Parthasarathi NL, Arvinth Davinci M, Utpal B, Jeevanantham AK. Determination of frictional coefficient of 316l (n) stainless steel by ring compression test using simulation. *J. Manuf. Eng.* 2018;13:113–7.
- [18] Vergne C, Boher C, Gras R, Levaillant C. Influence of oxides on friction in hot rolling: experimental investigations and tribological modelling. *Wear* 2006;260:957–75. <https://doi.org/10.1016/j.wear.2005.06.005>.
- [19] Zambrano OA, Gallardo KF, Polania DM, Rodríguez SA, Coronado JJ. The role of the counterbody's oxide on the wear behavior of HSS and Hi-Cr. *Tribol Lett* 2017;66:1. <https://doi.org/10.1007/s11249-017-0954-1>.
- [20] Graf M, Ullmann M, Korpala G, Wester H, Awiszus B, Kawalla R, Behrens B-A. Forming and oxidation behavior during forging with consideration of carbon content of steel. *Metals* 2018;8. <https://doi.org/10.3390/met8120996>.
- [21] Hardell J, Hernandez S, Mozgovoy S, Pelcastre L, Courbon C, Prakash B. Effect of oxide layers and near surface transformations on friction and wear during tool steel and boron steel interaction at high temperatures. *Wear* 2015;330–331:223–9. <https://doi.org/10.1016/j.wear.2015.02.040>.
- [22] Odabas D. The influence of the temperature on dry friction of AISI 3315 steel sliding against AISI 3150 steel. *IOP Conf Ser Mater Sci Eng* 2018;295:012021. <https://doi.org/10.1088/1757-899X/295/1/012021>.
- [23] Matsumoto R, Osumi Y, Utsunomiya H. Reduction of friction of steel covered with oxide scale in hot forging. *J Mater Process Technol* 2014;214:651–9. <https://doi.org/10.1016/j.jmatprotec.2013.10.011>.
- [24] Takeda M, Onishi T, Nakakubo S, Fujimoto S. Physical properties of iron-oxide scales on Si-containing steels at high temperature. *Mater Trans* 2009;50:2242–6. <https://doi.org/10.2320/matertrans.M2009097>.
- [25] Barrau O, Boher C, Vergne C, Rezai-Aria F, Gras R. In: *6th international tooling conference*. Karlstad, Sweden: KARLSTAD UNIVERSITY; 2002. p. 81–94.
- [26] Luong LHS, Heijkoop T. The influence of scale on friction in hot metal working. *Wear* 1981;71:93–102. [https://doi.org/10.1016/0043-1648\(81\)90142-3](https://doi.org/10.1016/0043-1648(81)90142-3).
- [27] Amano T, Okazaki M, Takezawa Y, Shiino A, Takeda M, Onishi T, Seto K, Ohkubo A, Shishido T. In: *Materials science forum*. Trans Tech Publ; 2006. p. 469–76. <https://doi.org/10.4028/www.scientific.net/MSF.522-523.469>.
- [28] Hutchings I, Shipway P. *Tribology: friction and wear of engineering materials*. second ed. Butterworth-Heinemann; 2017. p. 165–236. <https://doi.org/10.1016/B978-0-08-100910-9.00006-4>.
- [29] Chicot D, Mendoza J, Zaoui A, Louis G, Lepingle V, Roudet F, Lesage J. Mechanical properties of magnetite (Fe₃O₄), hematite (α -Fe₂O₃) and goethite (α -FeO·OH) by instrumented indentation and molecular dynamics analysis. *Mater Chem Phys* 2011;129:862–70. <https://doi.org/10.1016/j.matchemphys.2011.05.056>.
- [30] Seo M, Chiba M. Nano-mechano-electrochemistry of passive metal surfaces. *Electrochim Acta* 2001;47:319–25. [https://doi.org/10.1016/S0013-4686\(01\)00577-1](https://doi.org/10.1016/S0013-4686(01)00577-1).
- [31] Fischer-Cripps AC. *Nanoindentation*. New York, NY: Springer New York; 2004. p. 195–212. https://doi.org/10.1007/978-1-4757-5943-3_12.
- [32] Oliver WC, Pharr GM. An improved technique for determining hardness and elastic modulus using load and displacement sensing indentation experiments. *J Mater Res* 1992;7:1564–83. <https://doi.org/10.1557/JMR.1992.1564>.
- [33] Oliver WC, Pharr GM. Measurement of hardness and elastic modulus by instrumented indentation: advances in understanding and refinements to methodology. *J Mater Res* 2004;19:3. <https://doi.org/10.1557/jmr.2004.19.1.3>.
- [34] Lawrence SK, Adams DP, Bahr DF, Moody NR. Mechanical and electromechanical behavior of oxide coatings grown on stainless steel 304L by nanosecond pulsed laser irradiation. *Surf Coat Technol* 2013;235:860–6. <https://doi.org/10.1016/j.surfcoat.2013.09.013>.
- [35] Li YP, Onodera E, Matsumoto H, Chiba A. Correcting the stress-strain curve in hot compression process to high strain level. *Metall Mater Trans A* 2009;40:982–90. <https://doi.org/10.1007/s11661-009-9783-7>.
- [36] Kunogi M. A new method of cold extrusion. *Trans Jpn Soc Mech Eng C* 1957;23:742–9. <https://doi.org/10.1299/kikai1938.23.742>.
- [37] Male AT, Cockcroft MG. A method for the determination of the coefficient of friction of metals under conditions of bulk plastic deformation. *J Inst Met* 1964;93:38–46. [https://doi.org/10.1016/0043-1648\(66\)90161-x](https://doi.org/10.1016/0043-1648(66)90161-x).
- [38] Beddoes J, Bibby MJ. *Principles of metal manufacturing processes*. Butterworth-Heinemann Oxford; 1999. p. 99–137. <https://doi.org/10.1016/B978-034073162-8/50006-0>.
- [39] Sofuoğlu H, Gedikli H, Rasty J. Determination of friction coefficient by employing the ring compression test. *J Eng Mater Technol* 2000;123:338–48. <https://doi.org/10.1115/1.1369601>.
- [40] Kobayashi S, Oh S-I, Altan T. *Metal forming and the finite-element method*. New York: Oxford University Press; 1989. <https://doi.org/10.1093/oso/9780195044027.001.0001>.
- [41] Avitzur B. *Israel journal of technology*. ISRAEL: WEIZMANN SCI PRESS ISRAEL 8A HORKANIA STREET PO BOX 801, JERUSALEM 91007; 1964. p. 295–&.
- [42] Zhu Y, Zeng W, Ma X, Tai Q, Li Z, Li X. Determination of the friction factor of Ti-6Al-4V titanium alloy in hot forging by means of ring-compression test using FEM. *Tribol Int* 2011;44:2074–80. <https://doi.org/10.1016/j.triboint.2011.07.001>.
- [43] Lee J, Lee C, Kim B. Reverse analysis of nano-indentation using different representative strains and residual indentation profiles. *Mater Des* 2009;30:3395–404. <https://doi.org/10.1016/j.matdes.2009.03.030>.
- [44] Schütze M. Mechanical properties of oxide scales. *Oxid Metals* 1995;44:29–61. <https://doi.org/10.1007/BF01046722>.
- [45] Zambrano OA, Coronado JJ, Rodríguez SA. Tempering temperature effect on sliding wear at high temperatures in mottled cast iron. *Tribol Lett* 2015;57:19. <https://doi.org/10.1007/s11249-014-0462-5>.